Porphyrins. 39.[1] Ammine and Nitridoosmium Porphyrins. Ligand Effects on the Electronic Structure of Osmium Octaethylporphyrins

Artemis Antipas,[2a] Johann W. Buchler,[2b,d] Martin Gouterman,*[2a] and Paul D. Smith[2b,c]

Contribution from the Department of Chemistry, University of Washington, Seattle, Washington 98195, and the Institut für Anorganische Chemie, Technische Hochschule, D-51 Aachen, West Germany. *Received May 29, 1979*

Abstract: A unified theory is presented for the electronic structure of 13 osmium porphyrins Os(OEP)L(L′) (OEP = octaethylporphyrin; L,L′ = neutral or ionic ligands including NH_3, pyridine, N_2, CO, CS, NO, methoxide, nitride, oxide, and perchlorate). The 13 complexes are organized into a "back-bonding-charge transfer series" **1–13.** Along this series there is a reciprocation between equatorial back-bonding from Os(d_π) orbitals into P(π) (P = porphyrin) and axial back-bonding from Os(d_π) into L(π^*) or L′(π^*). For complexes lower in the series, **1–5**, equatorial back-bonding dominates, the (π,π^*) transitions are blue shifted owing to a π-bonding interaction between d_π and $e_g(\pi^*)$ orbitals, there are low-energy (d_π,π^*) charge-transfer (CT) transitions, and the metal is easily oxidized. With later members of the series axial back-bonding dominates, the (π,π^*) transitions are no longer blue shifted as back-bonding between d_π and ligand l_{π^*} orbitals dominates, so the energy of $e_g(\pi^*)$ levels is not affected, allowed charge transfer transitions (π,l_{π^*}) appear in absorption, and the metal is difficult to oxidize. The theory is based on new absorption spectra, new emission spectra, and iterative extended Hückel calculations. Absorption spectra are presented for Os(OEP)(NH_3)$_2$ (**1**), Os(OEP)CS(py) (**6**), Os(OEP)NO(F) (**8**), Os(OEP)(NO)$_2$ (**9**), Os(OEP)NO(O-ClO_3) (**10**), Os(OEP)N(OMe) (**11**) at 77 K, and Os(OEP)N($OClO_3$) (**13**) (py = pyridine, Me = methyl). We also report phosphorescence spectra at 77 K for **6** (661 nm, $\sim 3 \times 10^{-2}$, 33 μs), **8** (687 nm, 1.2×10^{-1}, 982 μs), **11** (732 nm, 3×10^{-2}, 195/74 μs), and **13** (742 nm, 1×10^{-2}, 65/21 μs). The numbers in brackets are origin wavelength, quantum yield, and exponential decay times; for **11** and **13** the decay is fit with two exponentials. We include a new report on the emission of Os(OEP)-O_2 (**12**) at 77 K (729 nm, 103/21 μs). All phosphorescences are from a triplet $T_1(\pi,\pi^*)$ level except for Os(OEP)CO(py) (**5**), which emits from a $T_1(d_\pi,\pi^*)$ level. The preparations of the first mononuclear nitridometalloporphyrins **11** and **13** by oxidation of the new bis(ammine) complex **1** are the major synthetic achievements described herein.

Introduction

The chemical and spectroscopic properties of metalloporphyrins have been the subject of much research work, some of which has been recently reviewed by the authors.[3-6] Also, recently, we have given considerable attention to the properties of Ru and Os complexes.[4,7-9] These complexes are of special interest because they are isoelectronic to the biologically important iron porphyrins. The Fe, Ru, and Os porphyrins show extremely variable electronic spectra depending on ligands, and a quantum-chemical explanation for this variability should be of great value for understanding the mechanism for the various biological activities of heme proteins. In this paper we shall present a general systematic interpretation for the electronic properties of 13 fully characterized osmium complexes of octaethylporphyrin, thus complementing our previous work.[4,7]

The 13 complexes to be discussed are listed in Table I. These complexes are all of form Os(OEP)L(L′), where $(OEP)^{2-}$, octaethylporphyrinate, acts as the equatorial ligand in a distorted octahedral complex, while L and L′ are the axial ligands on opposite sides of the porphyrin plane. The axial ligands are not only neutral molecules but also ions (nitrosonium, methoxide, fluoride, perchlorate, nitride, and oxide). For four complexes (**1**, **2**, **3**, and **12**) we have L = L′; however, for **9** we have L = NO^+ (linear) and L′ = NO^- (bent).[4,9b] The complexes have been listed from **1** to **13** on the basis of the red shift of the α or Q(0,0) band. Complexes **1–10** contain formally Os^{II} while **11–13** are derivatives of Os^{VI}. The 14th compound listed, Os(OEP)N(F) (**14**), is only characterized by its optical absorption spectrum. It behaves similar to **11** and is used as an analogue for the latter in the calculations. Complexes **7–14** show "two Soret bands", B_1 and B_2, in the regions of about 450 and 350 nm, respectively.

The purpose of this paper is to show that the wide variation in electronic properties of these 13 complexes can be largely comprehended in terms of a reciprocation between what we shall call *equatorial* back-bonding and *axial* back-bonding. By *equatorial* back-bonding we refer to delocalization from metal d_π to ring $e_g(\pi^*)$ orbitals, and by *axial* back-bonding we refer to delocalization from metal d_π to ligand l_{π^*} orbitals. We shall show that *equatorial* back-bonding decreases and *axial* back-bonding increases through the series **1–13**. A semantic point should be mentioned here. In crossing from **10**, which contains Os^{II}, to **11**, which contains Os^{VI}, "back-bonding" formally becomes "multiply dative covalent bonding". While the electrons populating the π-bonding orbitals formally belong to the metal atom in the Os^{II} complexes, they stem from the p orbitals of the axial ligands in the Os^{VI} complexes. However, the variation of electronic properties crosses this formal line smoothly.[4] We shall use the term "back-bonding" for the entire series. We shall apply this interpretation to explain the variation in the optical absorption and emission properties of the complexes listed in Table I. Further, we shall use iterative extended Hückel (IEH) calculations to provide theoretical justification for this view. It should be noted that other properties, such as infrared stretching frequencies for a series of CO or NO^+ complexes, NMR δ values for the methine hydrogen, and redox potentials, have been presented earlier[4] and fit the general trends rationalized by the model proposed here.

Experimental Section

Synthesis. References to the synthesis and chemical characterization of the compounds in Table I have been given earlier[4,7,8,9] except for the bis(ammine), nitrosyl, or nitrido complexes **1**, **10**, **11**, **13**, and **14**. Microanalyses were performed by Analytische Laboratorien (vormals A. Bernhardt), D-5250 Engelskirchen, West Germany.

Nitrosyl(octaethylporphinato)perchloratoosmium(II), Os(OEP)-NO($OClO_3$) (10). To a boiling solution of 55 mg (0.07 mmol) of Os(OEP)NO(OMe) (**7**) in 4 ml of CH_2Cl_2 was added a mixture of 4 mL of MeOH and 1 mL of $HClO_4$ (7% aqueous). After concen-

0002-7863/80/1502-0198$01.00/0

Table I. Specification and References for the Osmium Porphyrins Os(OEP)L(L′) **1–14**[e]

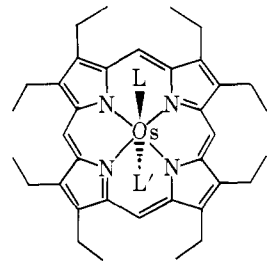

Os(OEP)L(L′) **1–14**

no.	L	L′	optical absorption, nm: α or Q(0,0)	optical absorption, nm: Soret	solvent	ref[b]
1	NH_3	NH_3	504	392	C_6H_6	*4, 8, c*
2	py	py	509	389	C_6H_6	*4, 7, 8*
3	$P(OMe)_3$	$P(OMe)_3$	522	406	CH_2Cl_2	*7, 9a*
4	N_2	THF	523	393	THF	*4, 7, 8*
5	CO	py	537	394	py	*4, 7, 8*
6	CS	py	544	396	3MP/py	*9c*
7	NO	OMe	567	**418**/337[d]	C_6H_6	*4, 7, 8, 9b*
8	NO	F	567	**415**/336	EPA	*4, 8, 9b*
9	NO	NO	576	423/350[a]	C_6H_6	*4, 8, 9b*
10	NO	ClO_4	581	424/365[a]	C_6H_6	*4, 8, c*
11	N	OMe	582	436/348	EPA	*4, 8, c*
12	O	O	594	438/**373**	MeOH	*4, 7, 8*
13	N	ClO_4	604	448/**355**	toluene	*4, 8, c*
14	N	F	580	439/**352**	C_6H_6	*c*

[a] Approximate value. [b] References given in italics either give the absorption peaks listed here or include an absorption spectrum. [c] This paper. [d] Boldface used when one Soret band is substantially more intense than the others. [e] Abbreviations: OEP^{2-} = octaethylporphyrinate; py = pyridine; Me = CH_3; THF = tetrahydrofuran; 3MP/py = 3-methylpentane/pyridine (20:1); EPA = ethyl ether/isopentane/ethanol (5:5:2).

tration of the solution to 4 mL and cooling, the dark red product separated. After filtration, rinsing with MeOH/H_2O (7:3), and drying at 80 °C (10^{-3} Torr), red needles of Os(OEP)NO($OClO_3$) (**10**, 54 mg, 90%) were obtained. Anal. Calcd for $C_{36}H_{44}N_5O_5ClOs$ (852.44): C, 50.72; H, 5.20; N, 8.22; O, 9.38; Cl, 4.16. Found: C, 51.21; H, 5.14; N, 8.29; O, 9.21; Cl, 3.92. IR (KBr): 1814 (NO^+);[4] 1174 (ClO_4^-); 645, 622, 598 cm^{-1} (ClO_4^- coordinated).

Bis(ammine)octaethylporphinatoosmium(II), Os(OEP)(NH_3)$_2$ (1). To a boiling solution of 50 mg (0.07 mmol) of Os(OEP)O_2 (**12**) in 8 mL of CH_2Cl_2 were added 5 mL of MeOH and subsequently 2 mL of hydrazine hydrate (100%). After concentration of the volume to 5 mL, blue-black crystals of **1** separated (36 mg, 72%). This air-sensitive product was filtered without recrystallization, washed with MeOH/H_2O (2:1), and dried at 80 °C (10^{-3} Torr). Anal. Calcd for $C_{36}H_{50}N_6Os$ (757.04): C, 57.12; H, 6.66; N, 11.10; O, 0.00. Found: C, 57.48; H, 6.72; N, 11.06; O, 0.18. IR: 3310, 3247 cm^{-1} (NH).

Nitrido(octaethylporphinato)perchloratoosmium(VI), Os(OEP)N($OClO_3$) (13). To a boiling solution of 111 mg (0.15 mmol) of Os(OEP)O_2 (**12**) in 15 mL of THF 0.2 mL of hydrazine hydrate (100%) was added dropwise. Thereafter the volume of the reaction solution was reduced to 5 mL by distillation and the remaining solvent removed under reduced pressure. The resulting crude, solid Os(OEP)(NH_3)$_2$ (**1**) was dried at 70 °C in vacuo for 1 h, redissolved in 10 mL of CH_2Cl_2/MeOH (1:1), and reacted with 0.2 mL of peracetic acid (~15% aqueous solution). The resulting solution was boiled until a color change from orange to red-green was observed. Then 0.5 mL of $HClO_4$ (7% aqueous) was added and the volume of the solution reduced to 4 mL by distillation. Shiny, black needles of crude Os(OEP)N($OClO_3$) (**13**) formed upon cooling. After washing with MeOH/H_2O (2:1), the product was recrystallized from a mixture of 10 mL of MeOH and 0.5 mL of $HClO_4$ (7% aqueous), yielding 90 mg (73%) of **13**. Anal. Calcd for $C_{36}H_{44}N_5O_4ClOs$ (836.44): C, 51.70; H, 5.30; N, 8.37; O, 7.65; Cl, 4.24. Found: C, 51.57; H, 5.32; N, 8.34; O, 7.49; Cl, 4.10. IR: 1142 (ClO_4^-); 1011 (OsN); 628, 618, 605 cm^{-1} (ClO_4^- coordinated).

Methoxonitrido(octaethylporphinato)osmium(VI), Os(OEP)N(OMe) (11). Recrystallization of 86 mg (0.10 mmol) of Os(OEP)N($OClO_3$) (**13**) from a solvent mixture consisting of 4 mL of CH_2Cl_2, 4 mL of MeOH, and 1 mL of KOH (1% aqueous) afforded fine, red needles of Os(OEP)N(OMe) (**11**, 65 mg, 82%) after washing with MeOH/H_2O (3:1) and drying at 70 °C (10^{-3} Torr). Anal. Calcd for $C_{37}H_{47}N_5OOs$ (768.02): C, 57.86; H, 6.17; N, 9.12; O, 2.08. Found: C, 57.78; H, 6.00; N, 9.15; O, 2.08. IR: 2765, 1080, 410 ($OMe^{3,4}$), 1008 cm^{-1} (OsN).

Fluoronitrido(octaethylporphinato)osmium (VI), Os(OEP)N(F) (14). A small sample of Os(OEP)N(OMe) (**11**) was dissolved in 6 mL of boiling acetone/CH_2Cl_2 (1:1) and treated with 0.5 mL of HF (40% aqueous). Black-green crystals of Os(OEP)N(F) (**14**) separated on cooling. Because this HF treatment normally introduces fluoride[9b,10] as a ligand and fluoride has about the same cis effect[4] on the optical spectrum as methoxide, e.g., in Os(OEP)NO(OMe) (**7**) and Os(OEP)NO(F) (**8**),[4,9b] the optical spectrum (benzene) seemed sufficient for the identification of **14**: λ_{max} (log ϵ) 580 (3.95), 550 (3.90), 439 (4.53), 352 (4.72) nm.

Optical Spectra. Absorption spectra reported here were taken either on a Cary 14 spectrophotometer or on a Unicam SP 800 B. Emission spectra, quantum yields, and lifetime measurements were carried out as described previously.[7,10] All the complexes of Table I, except **1**, were examined for emission in liquid nitrogen (77 K) in the spectral range 600–850 nm using an RCA 8852 photomultiplier tube. Excitation spectra showed that all reported emissions come from the main absorbing species. The compounds reported as nonemitting showed some weak peaks in the emission spectrum, but excitation spectra showed that these were not emissions from the main absorbing species. Some of the compounds could only be studied in snow-forming solvents due to instability in the glassy solvents tried; yields in these cases were obtained by comparison to Zn(Etio-I) (etioporphyrin I) also in a snow, and such yields are less accurate.

Iterative Extended Hückel (IEH) Calculations. The method and parameters for H, C, N, O, and Os have been explained previously.[7,11,12] The sulfur parameters are those used by Hanson et al.[13] for calculations on ferrous porphyrin complexes with CO and mercaptide. For fluorine the basis set exponentials were obtained by the method of Cusachs et al.,[14] and the ionization energies come from the tables of Basch, Viste, and Gray as presented by McGlynn et al.[15] The S and F parameters are given in Table II.

We did not do calculations on complexes **10** and **13**, because the perchlorate ligand geometry is not clear; the correct geometry,

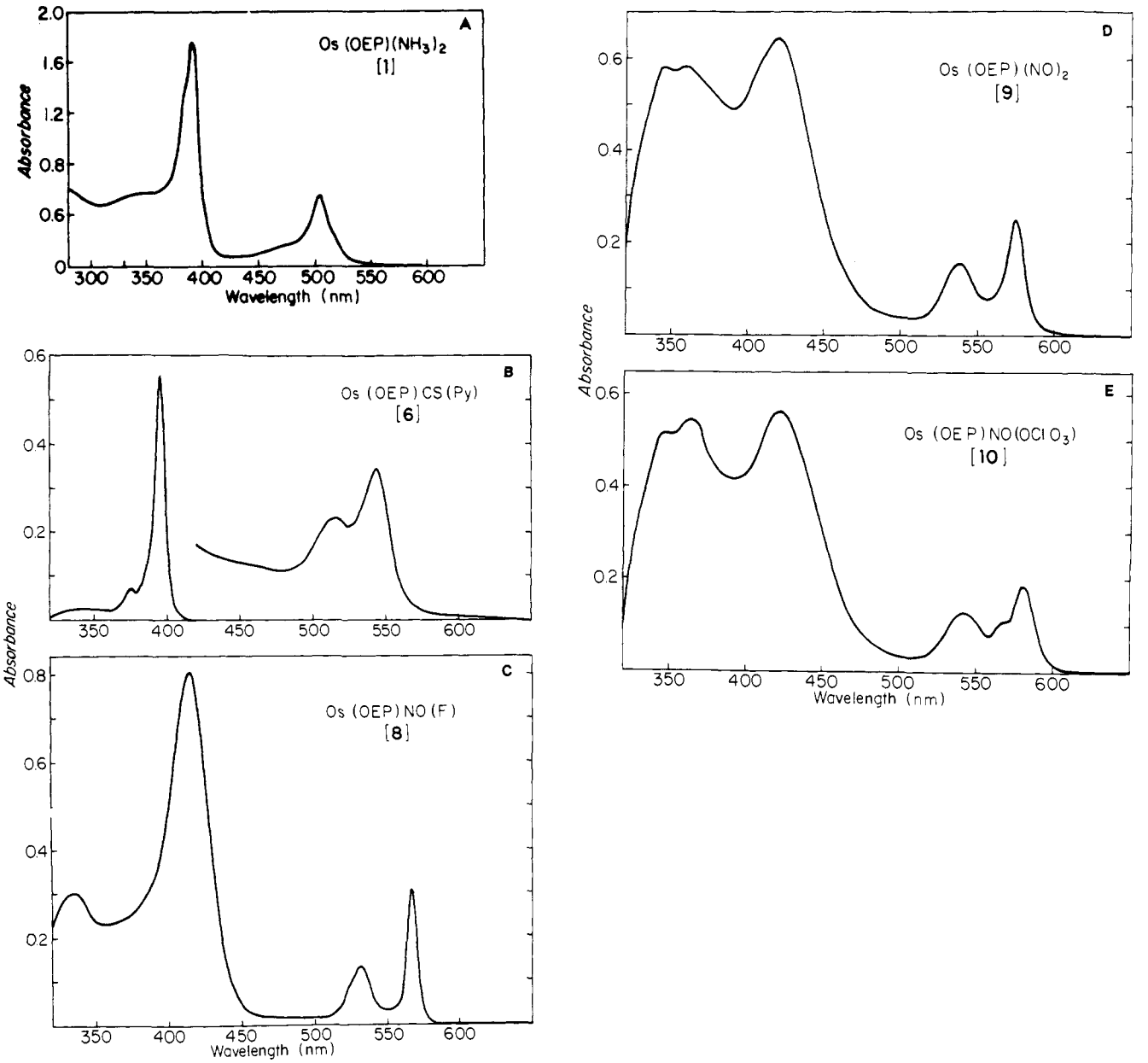

Figure 1. Absorbance vs. wavelength (nm) at room temperature of (A) $Os(OEP)(NH_3)_2$ (**1**), 1.8×10^{-5} M, in tetrahydrofuran; (B) Os(OEP)CS(py) (**6**) in 3-methylpentane/pyridine (~20:1); (C) Os(OEP)NO(F) (**8**) in EPA [ethyl ether/isopentane/ethanol (5:5:2)]; (D) $Os(OEP)(NO)_2$ (**9**) in EPA; (E) $Os(OEP)NO(OClO_3)$ (**10**) in benzene.

Table II. Iterative Extended Hückel Parameters[a]

atom	ionization energies, eV	exponents, au^{-1}
S^-, S, S^+	s: 11.1, 20.3, 33.8	2.1223
	p: 2.1, 10.4, 23.4	1.8273
F^-, F, F^+	s: 18.1, 40.12, 69.1	2.50
	p: 2.38, 18.94, 42.45	2.21

[a] For other atoms see ref 7 and 11.

moreover, is likely to lower the symmetry, thus increasing the cost of the IEH calculations. To model the electronic structures of **10** and **13**, we calculated the monocations $Os(OEP)NO^+$ (**10a**) and $Os(OEP)N^+$ (**13a**), respectively. In view of the high NO stretching frequency of **10** (see Experimental Section), it seemed justified to take **10a** instead of **10** and then **13a** instead of **13** because the nitridoosmium(VI) system is so closely related to the nitrosylosmium(II) system.[4] We also had some difficulty with the convergence of our calculations on **11**, being hindered by the low symmetry of the methoxide and by the fact that oxygen ligands sometimes give spuriously high energies of occupied orbitals.[7,16] In this case we modeled the molecule as Os(OEP)N(F) (**14**) for the calculations. This is again justified by the close spectral relationships of **11** and **14**, or **7** and **8**,[9b] respectively (see Table I).

Table III. Key Bond Lengths (Å) and Bond Angles (deg)[a,b]

compd	bond lengths and angles
1	Os-N = 2.10; NH = 1.09; ∠HNH = 110
6	$Os-N_{py}$ = 2.10;[c] Os-C = 1.72; CS = 1.53; ∠OsCS = 180
8	Os-N = 2.00; Os-F = 1.97; N-O = 1.16; ∠OsNO = 180
9	∠OsNO = 180; Os-N = 2.00; N-O = 1.16
	∠OsNO = 127; Os-N = 1.98; N-O = 1.24
10a	Os-N = 1.80; N-O = 1.13
12	Os-O = 1.86[d]
13a	Os-N = 1.80
14	Os-N = 1.80; Os-F = 1.97; ∠NOsF = 180

[a] The Os porphine moiety is planar with ring coordinates given earlier[7] and $Os-N_p$ = 2.049 Å. [b] IEH results quoted for **2–5** and **7** are taken from earlier calculations.[7] [c] The geometry for pyridine was given previously.[7] [d] A distance of 1.80 Å was used previously.[7]

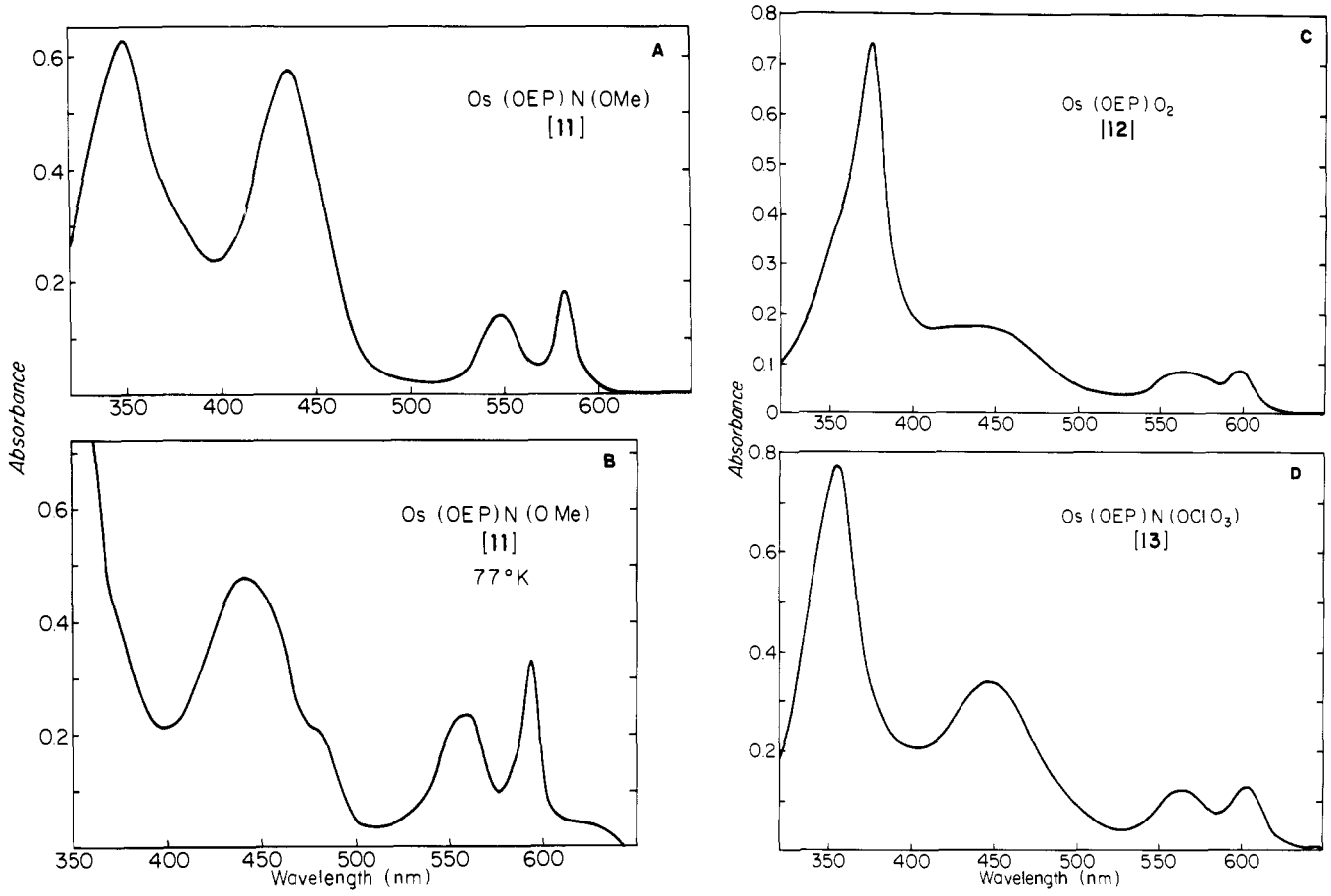

Figure 2. Absorbance vs. wavelength (nm) of (A) Os(OEP)N(OMe) (**11**) in EPA at room temperature; (B) **11** in EPA at 77 K; (C) $Os(OEP)O_2$ (**12**) in toluene at room temperature; (D) $Os(OEP)N(OClO_3)$ (**13**) in toluene at room temperature.

In all calculations, the orientation of the porphyrin molecules with respect to the coordinate axes was such that the center of the coordinate system coincides with the center of the porphyrin plane and the nitrogens are on the x, y axes. All atoms are in the x, y plane except for those of the axial ligands L, L′. The calculations were done on the unsubstituted porphine ring (P), having the "D_{4h}-planar projected" geometry used previously,[11] with the Os-N_p distance set at 2.049 Å in all complexes. Other important geometrical parameters are given in Table III.

Results and Discussion

Optical Spectra. Absorption. Based on the optical absorption spectra, we have listed the Os complexes **1–13** in Table I in the order of increasing wavelength of the α band. The optical spectra of many of these complexes have been reported earlier, as indicated in Table I. In Figure 1 we show the absorption spectra of five Os^{II} complexes. The spectra of **1**, **8**, and **10** have not previously been published. In Figure 2 we show spectra of three Os^{VI} complexes of Table I. The data in Table IV on absorption were taken from the spectra of Figure 1 for complexes **1**, **6**, and **8**, while the tabular data for the other complexes were taken from the spectral runs of Smith.[8,9b,c]

As discussed earlier,[4-7] porphyrin optical spectra in the visible-near-UV region fall into three main classes: *normal* spectra show the (π,π^*) bands Q, B, N in order of increasing energy; *hypso* spectra are similar but blue shifted; *hyper* spectra show strong extra allowed bands. As pointed out earlier,[4,7] complexes of the type Os(OEP)L(L′) show a mixed *hypso/hyper* character. We now detail how this character varies through the series of complexes **1–13**.

The most extreme hypso spectra are shown by the bisammine (**1**) and bispyridine (**2**) complexes. In addition to the normal (π,π^*) bands, the spectrum of **2** shows very clear extra bands in the visible-near-UV absorption spectrum;[7] while not so prominent, the spectrum of **1** (Figure 1A) also shows extra bands as shoulders at ~383, ~472, ~517, and a tail ~540 nm. In these two complexes the extra bands are attributed to allowed doubly excited states with configuration $[e_g(d_\pi)]^3[a_{1u}(\pi), a_{2u}(\pi)]^3[e_g(\pi^*)]^2$; forbidden charge-transfer (CT) states $[e_g(d_\pi)]^3[e_g(\pi^*)]$ are observed in the near-infrared spectrum of **2**.[7]

For complexes **3–6**, the absorption spectrum shows no obvious extra bands. However, Os(OEP)CO(py) (**5**) shows evidence for forbidden CT states $[e_g(d_\pi)]^3[e_g(\pi^*)]$ in the visible region in the observed broadening of the Q bands;[7] the related complex Ru(OEP)CO(py) shows evidence for these forbidden CT states in a prominent tail to the red of the Soret bands.[7] The spectrum of Os(OEP)CS(py) (**6**) (Figure 1B) shows both these effects, attributed to the presence of forbidden CT excited states in the visible region.

Complexes **7–13** differ from compounds **1–6** (see Table I) by showing two Soret bands, which we label B_2 and B_1 in Table IV. Through the series **7–13**, the Soret bands suffer a red shift and the extinction coefficient of the shorter wavelength B_2 increases at the expense of the longer wavelength B_1. The Q(0,0) or α band also shifts to the red. Thus for **7** and **8** the intensity of the B_2 band is sufficiently weak that the hyper character of the spectrum is not fully apparent; for these complexes the α bands are at sufficiently high frequency that the spectra are still of the hypso type. However, by **9** the hyper character of the spectrum is clear in the presence of two comparably intense Soret bands; for these complexes the α band is now shifted so far to the red that the label hypso is inappropriate.

A striking feature of the spectral changes among these

Table IV. Electronic Absorption Maxima (nm) and Absorbance[a,b]

compd	no.	solvent	B_2[c]	B_1[c]	other	Q(1,0)	Q(0,0)
$Os(OEP)(NH_3)_2$	**1**	C_6H_6	[352 sh]	392		475 sh	504
			(4.488)	(4.980)		(3.964)	(4.486)
Os(OEP)CS(py)	**6**	3MP/py	[~350, 375]	396	~460	514	544
			(4.46)	(5.36)		(4)	(4.15)
Os(OEP)NO(F)	**8**	EPA	336	415		532	567
			(4.40)	(4.81)		(4)	(4.40)
$Os(OEP)(NO)_2$	**9**	C_6H_6	350	423		539	576
			(4.651)	(4.705)		(4.119)	(4.218)
$Os(OEP)NO(OClO_3)$	**10**	C_6H_6	365	424		543	580
			(4.707)	(4.703)		(4.098)	(4.283)
Os(OEP)N(OMe)	**11**	CH_2Cl_2	357	435		545	578
			(4.644)	(4.777)		(4.169)	(4.274)
$Os(OEP)O_2$	**12**	MeOH	373	438		556	594
			(4.879)	(4.386)		(4.032)	(4.092)
$Os(OEP)N(OClO_3)$	**13**	THF	357	448		567	605
			(4.857)	(4.472)		(3.983)	(4.036)

[a] We give either log a (relative absorbance) or log ϵ (molar extinction) in parentheses. The former numbers are scaled so log $a = 4$ for the Q(1,0) band. [b] Abbreviations as in Table I. Also, sh ≡ shoulder. [c] Complexes **8–13** show two Soret bands that we label B_1 and B_2. For **1** and **6** the bands in brackets are not second Soret bands. See text.

complexes is the great similarity between the spectrum of $Os(OEP)NO(OClO_3)$ (**10**) (Figure 1E) and Os(OEP)N(OMe) (**11**) (Figure 2A), which contain Os^{II} and Os^{VI}, respectively. The close relationship of the nitrosylosmium(II) and nitridoosmium(VI) species has already been discussed;[4] here, it seems that small remaining differences in the cis effects of the nitrosyl or nitrido systems are compensated by the different cis effects of methoxo or perchlorato ligands on the optical spectrum of the osmium porphyrin. Another interesting feature is a striking temperature dependence of the absorption spectrum of **11**. As shown in Figures 2A and 2B, the effects of decreased temperature on **11** are a red shift of the spectrum and an increase of the intensity ratio of B_2/B_1. Thus the effect of lower temperature is to make the spectrum of **11** more like that of **12** (Figure 2C) or **13** (Figure 2D). A similar temperature dependence has been reported for Fe(TPP)NO(Cl).[17]

Emission. In a previous paper[7] we reported emission studies on six of the complexes of Table I. We found that complexes **2–4** have no emission, that **5** emits from a lowest triplet of CT character, i.e., $T_1(d_\pi,\pi^*)$, that **7** emits from a $T_1(\pi,\pi^*)$ state, and that **12** emits from a T_1 state substantially red shifted from the usual ring $T_1(\pi,\pi^*)$ emission. We have now extended emission studies at 77 K to include complexes **2–13** of Table I. (Our previous study of **12** was done at room temperature in a degassed solution.[7])

Before discussing the new emission data, we should mention our negative findings. We could find no emission from $Os(OEP)(NO)_2$ (**9**) nor from $Os(OEP)NO(OClO_3)$ (**10**). Also we found no fluorescence mirror image to the first absorption band for any of the complexes studied. These negative results can be taken as establishing an upper limit for such emission yields as $\Phi_{em} < 3 \times 10^{-4}$.

Figure 3 gives emission spectra for Os(OEP)CS(py) (**6**) and Os(OEP)NO(F) (**8**), and Figure 4 gives emission spectra for the three Os^{VI} complexes, **11–13**; all spectra were taken at 77 K. Table V lists the emission peaks for these spectra, and Table VI summarizes the emission data for the seven Os(OEP)L(L′) complexes found to emit. One of these emissions, that of Os(OEP)CO(py) (**5**), we characterize as coming from a $T_1(d_\pi,\pi^*)$ excited state and all the others as coming from a $T_1(\pi,\pi^*)$ excited state. This difference is manifest in three emission properties: (1) The energy gap between Q(0,0) and $T_1(0,0)$ ($E_Q - E_T$ in Table VI) is anomalously large for **5**, while that for the other complexes is comparable to the energy gap observed for a variety of other metal octaethylporphyrin complexes.[10,18-20] (2) The lifetime of **5** is anomalously short,

Table V. Emission Peaks for Os Complexes at 77 K[a]

compd	no.	solvent	phosphorescence peaks, nm
Os(OEP)CS(py)	**6**	3MP/py	661, 712, ~734
Os(OEP)NO(F)	**8**	EPA	687, 718, 745, ~756, 771
Os(OEP)N(OMe)	**11**	EPA	732, 797, ~814
$Os(OEP)O_2$	**12**	toluene	729, 768, ~803, ~823
$Os(OEP)N(OClO_3)$	**13**	toluene	742, ~810

[a] Abbreviations as in Table I.

whereas the lifetime of the other complexes of Table VI is roughly comparable to the 120-μs lifetime observed for Pt(Etio-I),[18] a porphyrin complex with a comparably heavy metal. (3) The emission spectrum of **5** is much broader and less structured than that of the other emitting complexes of Table VI.

The six complexes of Table VI that emit from $T_1(\pi,\pi^*)$ levels show considerable variation among themselves. They fall into three subclasses.

(A) The emission of Os(OEP)CS(py) (**6**) is anomalously broad (Figure 3A), although not so broad as the emission of **5**,[7] and its lifetime is anomalously short, but again not so short as that of **5**. The two vibronic bands of **6**, at 1080 and 1500 cm^{-1}, are unusually intense; we found that all three bands show the same decay rate. Qualitatively, the emission spectrum of **6** is intermediate between that of Ru(OEP)CO(py), which emits from $T_1(\pi,\pi^*)$, and that of Os(OEP)CO(py), which emits from $T_1(d_\pi,\pi^*)$.[7] We tend to ascribe the peculiarities in the emission of **6** to the presence of a state $T_1(d_\pi,\pi^*)$ slightly above the emitting $T_1(\pi,\pi^*)$ level, which perturbs the emission spectrum and lifetime.

(B) The emission spectra of Os(OEP)NO(OMe) (**7**)[7] and Os(OEP)NO(F) (**8**) (Figure 3B) are quite similar and are rather like phosphorescence spectra generally observed from $T_1(\pi,\pi^*)$ excited states of d^0 or heavier d^6, d^8, or d^{10} metal octaalkylporphyrin complexes[10,18-20] in having a sharp, intense origin band and several clear vibronic bands of much lower intensity. In all the systems mentioned the d_π orbitals are either empty or at rather low energy. The emission of **8** has a remarkably long lifetime and high quantum yield; the shorter, nonexponential decay of **7** and its much lower quantum yield suggest that **7** differs from **8** only in a greatly enhanced radiationless decay.

Table VI. Os(OEP)L(L') Triplet State Properties[a]

compd	no.	solvent	ϕ_p	τ_p,[b] μs	$\lambda_p(0,0)$, nm	$E_Q - E_T$,[c] cm^{-1}
Os(OEP)CO(py)	**5**	3MP	6×10^{-4}	<6	~720	4980
Os(OEP)CS(py)	**6**	3MP/py	$\sim 3 \times 10^{-2}$	23	661	3030
Os(OEP)NO(OMe)	**7**	3MP	3×10^{-3}	116/35	688	3140
Os(OEP)NO(F)	**8**	EPA	1.2×10^{-1}	982	687	3070
Os(OEP)N(OMe)	**11**	EPA	3×10^{-2}	195/74	732	3050
$Os(OEP)O_2$	**12**	toluene		103/21	729	3120
$Os(OEP)N(OClO_3)$	**13**	toluene	$\sim 1 \times 10^{-2}$	65/21	742	3200

[a] Abbreviations as in Table I. All emissions at 77 K. [b] Entries such as 116/35 indicate τ_1/τ_2 for nonexponential decays fit as $A_1e^{-t/\tau_1} + A_2e^{-t/\tau_2}$. [c] Energy gap between Q(0,0) absorption and $T_1(0,0)$ emission.

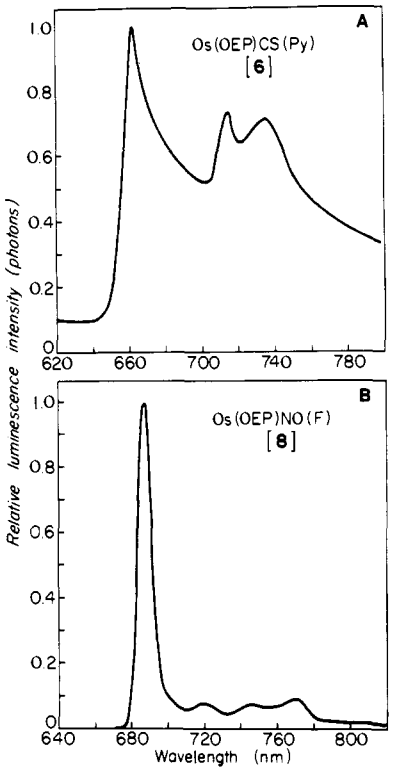

Figure 3. Emission spectra at 77 K of (A) Os(OEP)CS(py) (**6**) in 3-methylpentane/pyridine (20:1); (B) Os(OEP)NO(F) (**8**) in EPA. Intensity proportional to photons per unit wavelength.

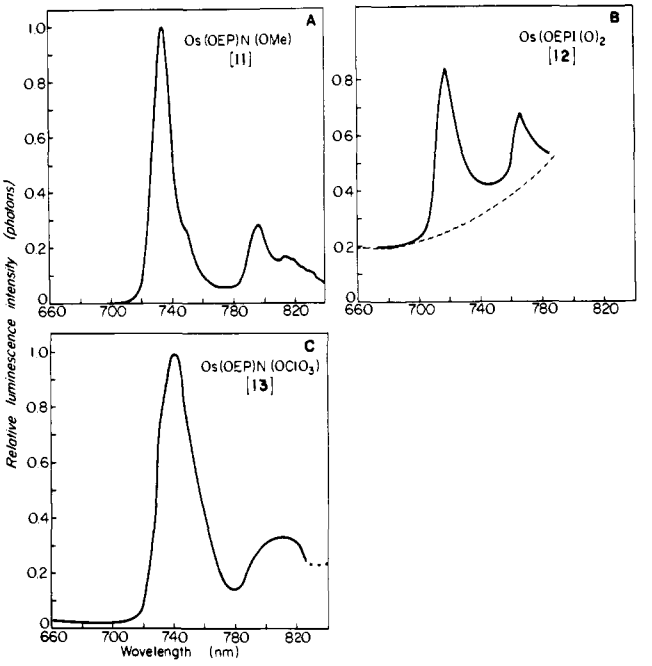

Figure 4. Emission spectra at 77 K of (A) Os(OEP)N(OMe) (**11**) in EPA; (B) $Os(OEP)O_2$ (**12**) in toluene; the high base line (dashed) due to solvent being a snow; (C) $Os(OEP)N(OClO_3)$ in EPA. Intensity proportional to photons per unit wavelength.

(C) The three Os^{VI} complexes, **11–13**, show comparable spectra (Figure 4), which are rather red shifted in keeping with the red shift of their Q(0,0) bands. All three have comparable double lifetimes. The emission spectra of **11–13** differ from those of **7** and **8** in vibronic structure. Thus **11**, **12**, and **13** show fairly intense vibronic bands, relative to $T_1(0,0)$, at 1130, 700, and 1110 cm^{-1}, respectively; on the other hand, **8** (Figure 3B) has three vibronic bands of comparable intensity at 630, 1130, and 1590 cm^{-1}, all of which are weak relative to $T_1(0,0)$. Thus the Os^{VI} complexes each show one vibronic band of lower wavenumber with enhanced intensity.

Qualitative Theory. We have in previous work[4,8] attempted qualitative interpretation of the electronic structure of osmium porphyrins, and we have also given results from IEH calculations.[7] The additional optical studies and further IEH calculations reported here allow a clear, unified interpretation for the variations in electronic structure across the series of complexes of Table I. Across this series there are regular changes in the pattern of back-bonding (BB) and in the energy of the charge-transfer (CT) transitions, so we shall refer to **1–13** as the BB-CT series. The theory for the BB-CT series was inspired by examining IEH calculations in comparison to optical data. But because the IEH model is only semiquantitative, it is useful to present an overview of the model and then show how the IEH calculations support the model.

The optical spectra and redox properties depend on the orbitals in the Fermi energy region, the Fermi energy being defined as in solid-state physics.[21] For normal porphyrins the important orbitals in the Fermi energy region are the two highest occupied molecular orbitals [HOMOs, $a_{1u}(\pi)$ and $a_{2u}(\pi)$] and the two lowest unoccupied molecular orbitals [LUMOs, $e_g(\pi^*)$].[6] In Fe, Ru, and Os porphyrins the electronic properties are complicated by the presence of metal d orbitals in the Fermi energy region; these d orbitals are, in turn, greatly affected by interaction with the orbitals of the axial ligands.

There are important "metal effects"[4] along the Fe, Ru, Os series. First, the orbitals 4d and 5d of Ru and Os are of comparable size, which is larger than the 3d orbitals of Fe. As a consequence the energy splitting between the three orbitals d_{xy}, d_{xz}, d_{yz} and $d_{x^2-y^2}$, d_{z^2} rises in the order Fe $\ll$ Ru $\lesssim$ Os.[7] This is shown theoretically by IEH calculations,[7] and experimentally by the fact that Fe^{II} porphyrins, but neither Ru^{II} nor Os^{II} porphyrins, show high spin.[6] For Ru and Os porphyrins $d_{x^2-y^2}$ and d_{z^2} are high enough in energy that they can be considered above the Fermi energy region. Because of the larger size, the $d_\pi \equiv d_{xz}$, d_{yz} orbitals of Ru and Os have greater *equatorial* back-bonding to the porphyrin orbital $e_g(\pi^*)$ and greater *axial*

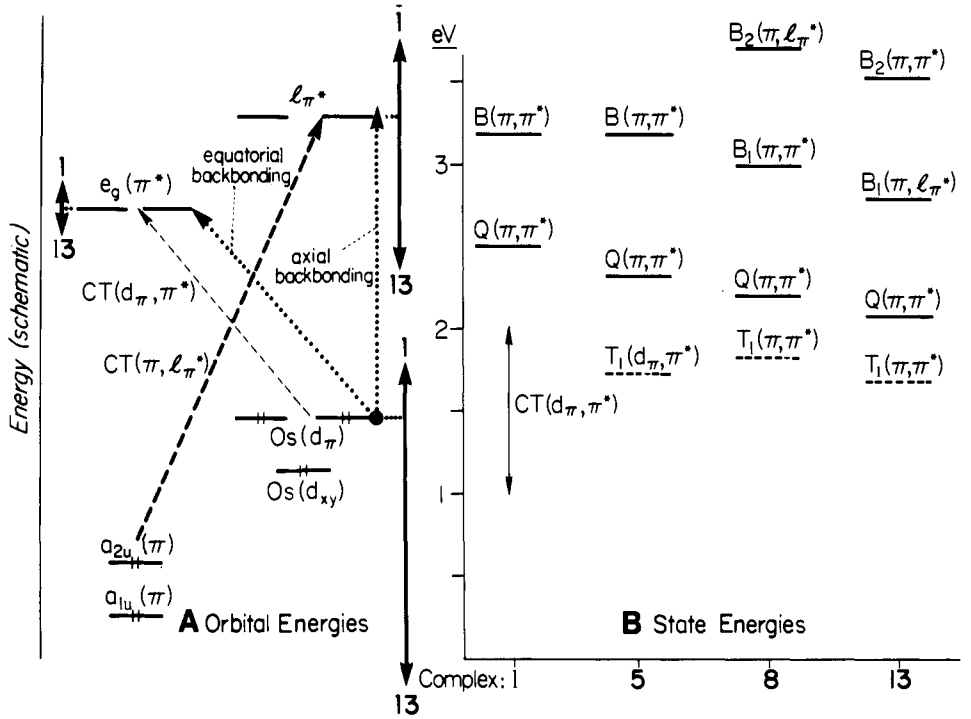

Figure 5. (A) Schematic diagram showing orbital energy shifts (vertical solid lines) among complexes Os(OEP)L(L'), **1–13**. Equatorial and axial back-bonding shown by dotted lines. Forbidden (light dashed line) and allowed (heavy dashed line) charge transfer (CT) transitions are shown. (B) State energies for selected complexes (data from Tables I and VI).

Table VII. π Electron Densities

no.	L	L'	P(π)[a]	L(π)	L(π)'	M(d_π)[b]	total[c]	(valence electrons)[c]	M(p_z)[b]
1	NH_3	NH_3	26.394			3.564	29.959	(30)	0.074
2	py	py	26.298	6.058	6.058	3.526	41.940	(42)	0.107
3	$P(OMe)_3$	$P(OMe)_3$	26.538			3.347	29.885	(30)	0.302
4	N_2	THF	26.170	4.508		3.323	34.001	(34)	0.172
5	CO	py	26.132	4.736	6.026	3.141	40.035	(40)	0.213
6	CS	py	26.166	4.625	6.032	3.181	40.004	(40)	0.192
8	NO	F	25.932	5.438	3.796	2.833	37.999	(38)	0.242
10a	NO^+		25.664	5.364		2.792	33.820	(34)	0.241
14	N	F	25.880	1.850	3.728	2.558	34.016	(34)	0.266
12	O	O	25.836	2.740	2.740	2.596	33.912	(34)	0.237
13a	N^+		25.544	2.023		2.453	30.020	(30)	0.279
15[d]			25.836			3.992	29.828	(30)	0.176
16[d]			25.912			3.994	29.906	(30)	0.094
17[d]			25.880			3.994	29.874	(30)	0.123

[a] Porphine ring. [b] Metal orbitals. [c] Total of columns 4–7; integer number of valence electrons in parentheses. [d] All atoms in plane. See ref 1: **15**, Cu instead of Os; **16**, Ag instead of Os; **17**, Ag^+ instead of Os (see Table I).

back-bonding to any vacant l_{π^*} orbital on a fifth or sixth ligand. Finally we note that the energy of the d_{xy}, d_π orbitals is Fe ~ Os > Ru.[7] The net result of these metal effects is a close resemblance of Ru and Os porphyrins, with the latter somewhat more like Fe porphyrins than the former owing to the closer similarity of their energies for d_{xy}, d_π.

Figure 5A shows the important orbitals in the Fermi energy region for the complexes Os(OEP)L(L') of Table I, and we shall discuss now how these orbitals vary in energy across the BB–CT series. The d_π orbital is quite high for **1**, whose ligands L = L' = NH_3 are σ donors with no π-acceptor capacity. As a result of the high d_π energy, *equatorial* back-bonding is strong, the (d_π,π^*) CT states are low in energy, back-bonding repulsion of d_π to $e_g(\pi^*)$ causes a strong hypsochromic shift to the (π,π^*) spectrum, and Os^{II} is easily oxidized with $E_{1/2}$ = −0.60 V.[4] With L = L' = py (**2**), the ligand has an l_{π^*} orbital; weak *axial* back-bonding lowers the energy of d_π and reduces *equatorial* back-bonding. As a result the (π,π^*) spectra are less hypsochromic, and Os^{II} is less easily oxidized with $E_{1/2}$ = −0.37 V.[4] *Axial* back-bonding increases through the complexes **3–6**. By **7** the l_{π^*} level has come so low in energy that the resulting increase in *axial* back-bonding dramatically reduces the energy of the d_π level which in turn leads to a decrease in *equatorial* back-bonding. The (π,π^*) spectra are just slightly hypsochromically shifted, and both **7** and **8** show hyper spectra due to an allowed CT transition (π,l_{π^*}). The redox potentials for **7** and **8** are $E_{1/2}$ = +0.92 and +1.00 V, respectively, and are probably ring oxidation; thus the metal oxidations are at even higher voltages.

In the Os^{VI} complexes, **11–13**, the empty metal d_π orbitals are combined with the filled, relatively low energy p_x, p_y orbitals on the axial ligand atoms resulting in a strong dative bond. The filled orbital of these bonds have substantial metal d_π character, and in some sense the Os^{VI} ion can be regarded as reduced to Os^{II}. The similar electronic properties of the nitrosylosmium(II) and the nitridooxmium(VI) systems are

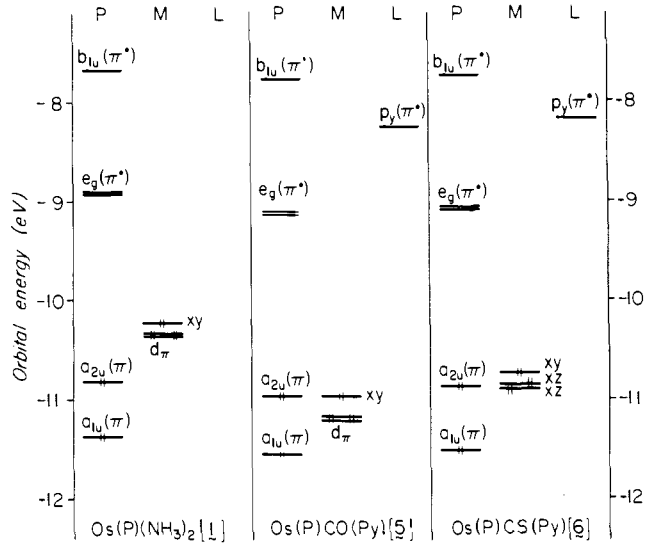

Figure 6. Energies of top filled and lowest empty MOs calculated by the iterative extended Hückel method for complexes Os(P)L(L') **1**, **5**, and **6**. The MOs are grouped as P, M, L depending on whether the electron density for the MO is largely porphine ring (P), metal (M), or ligand (L). D_{4h} symmetry labels are used.

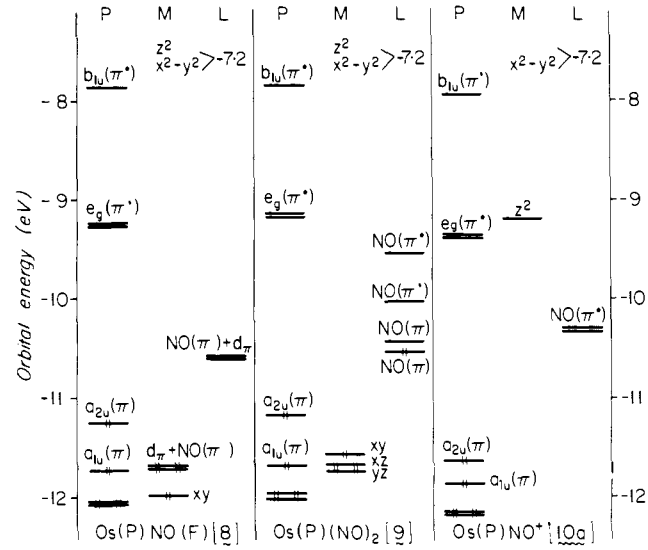

Figure 7. Energies of top filled and lowest empty MOs for complexes Os(P)L(L') **8** and **9** and for Os(P)NO$^+$ (**10a**). The orbitals are presented as in Figure 6.

manifest in the IEH calculations (Table VII, below), which show a relatively small decrease in d_π population between complexes **8** (Os^{II}) and **14** (Os^{VI}). For **11–13** the CT transitions (π,l_{π^*}) are low in energy. These transitions can interact with the normal B(π,π^*) and Q(π,π^*) ring states because they have the same symmetry. When the CT(π,l_{π^*}) states lie above the Soret band, B_2 is less intense than B_1; when the CT transitions are below the Soret band, B_2 is more intense than B_1. We see in Table IV that B_2 is less intense than B_1 for **11**, but more intense for **12** and **13**. As the CT transitions become lower, we expect them to interact with the Q(π,π^*) levels, pushing them to the red, as is observed for **11–13**.

While Figure 5A shows the shifting of orbital energies through the series of Os(OEP)L(L') complexes of Table I (idealizing the trends found in the IEH calculations presented below), it should be stressed that the orbital energy differences on a single energy diagram cannot correctly represent both (π,π^*) and CT states because of their different electron interaction energy. To emphasize this, Figure 5B shows the energy for the (π,π^*) and CT excited states identified for complexes **1**, **5**, **8**, and **13**.

These same considerations allow us to rationalize emission properties along the BB-CT series. The lack of emission of **2–4**[7,22] we attribute to low-energy CT states (d_π,π^*) that provide paths for radiationless decay to the ground state. By **5** these CT states have become high enough in energy so that emission comes from a T_1(d_π,π^*) excited state. Complexes **6–8** show emission from T_1(π,π^*) levels as do **11–13**. (Reasons for the lack of emission from **9** and **10** are discussed in the next section.) Furthermore, we might expect spin-orbit coupling to decrease from **6** to **8** and to increase from **11** to **13**. In **6–8** the spin-orbit coupling is set by the extent of back-bonding between d_π and $e_g(\pi^*)$, which decreases along this series. In **11–13** the spin-orbit coupling is set by the configuration interaction between the normal T_1(π,π^*) level and T(π,l_{π^*}) CT levels, which increase along this series. Because l_{π^*} is antibonding between ligand π^* and metal d_π, increased T(π,l_{π^*}) character should increase spin-orbit coupling. (While emission lifetimes depend on radiationless as well as radiative decay rates, to some extent both will increase together with increased spin-orbit coupling. Thus an argument based on the size of the spin-orbit effect can relate to observed decay rates, although this may not always be true.)

Finally we note that, although d_{xy} appears in Figure 5, explicit effects of this orbital are not clear experimentally. Calculations (next section) show that the energy of d_{xy} remains near that of d_π throughout the BB-CT series. Of course only d_π displays back-bonding, and d_{xy} remains relatively pure because of symmetry. We have given evidence[7] for low-energy CT transitions in complexes **1–6**, which we refer to as (d_π,π^*) because generally the d_π orbitals are strongly interacting. However, there may be (d_{xy},π^*) transitions in the same energy region, which the data does not yet distinguish.

IEH Calculations. Figures 6–8 show orbital energy calculations for complexes **1**, **5**, **6**, **8**, **9**, and **12**. As explained above, in place of **10**, **11**, and **13**, we give plots for **10a**, **14**, and **13a**. Plots for **2–5**, **7**, **8**, and **12** have appeared earlier.[7]

Figure 6 shows early members of the BB-CT series. As discussed qualitatively above, we see that the d_{xy}, d_π levels shift to lower energy from **1** to **5** and **6**; l_{π^*} orbitals are absent in **1** and remain high in energy in **5** and **6**. We might note that the energy gaps between $e_g(\pi^*)$ and the average of $a_{2u}(\pi)$ and $a_{1u}(\pi)$ are 2.18, 2.14, and 2.11 for **1**, **5**, and **6**, respectively; thus the IEH calculations qualitatively give the observed red shift (Table I). Note also that Figure 6 shows that the first oxidation occurs at the metal in **1**, whereas metal and ring oxidations are predicted to be of comparable energy in **5** and **6**.

Figure 7 shows three nitrosonium complexes. The filled orbitals d_{xy}, d_π are low in energy. But now (π,l_{π^*}) transitions are expected. It should be noted that quite generally IEH calculations are expected to underestimate the energy for CT transitions,[23] so the energy for l_{π^*} in the diagram is reasonable. A red shift of (π,l_{π^*}) between **7** and **8** is predicted. The levels of **9** are complicated by having one HOMO on NO^- and three LUMOs on NO^+ and NO^-. Low-energy transitions among the NO filled and empty orbitals could provide paths for radiationless decay, thus explaining the lack of emission of **9**. The ion **10a** used to model **10** would appear to have NO(π^*) at higher energy, which may be an artifact of the cation model. It should be noted that the NO stretching frequency takes values of 1745, 1770, 1778, and 1814 cm^{-1} along the series **7–10**,[7] thus showing decreased back-bonding into l_{π^*}. If σ donation decreases along the series OMe^-, F^-, $OClO_3^-$, the d_π orbitals will drop in energy, thus having less back-bonding to l_{π^*}. Experimentally it appears that reduced back-bonding to l_{π^*} goes together with lower energy for the CT(π,l_{π^*}) levels. The lack of emission of **10** may come about because the lowest

Table VIII. Calculated Total Charge Densities and Selected Experimental ^{1}H NMR data (P = Porphine, M = Metal)

no.	L	L′	P	M	L	L′	δ_{meso}[a]
1	NH_3	NH_3	−0.842	0.212	0.315	0.135	*b*
2	py	py	−0.730	0.220	0.255	0.255	8.48[c]
3	$P(OMe)_3$	$P(OMe)_3$	−0.969	0.172	0.399	0.399	9.10
4	N_2	THF	−0.450	0.271	−0.122	0.299	*b*
5	CO	py	−0.345	0.282	−0.199	0.271	9.64
5a[d]	CO	py	−0.344	0.271	−0.167	0.240	9.93
6	CS	py	−0.474	0.255	−0.016	0.235	10.01
7	NO	OMe	−0.104	0.358	−0.147	−0.107	10.45
8	NO	F	0.067	0.373	−0.047	−0.393	10.41
9[e]	NO^+	NO^-	−0.086	0.345	−0.116	−0.143	10.46
10a	NO^+		0.499	0.424	0.077		10.40[f]
14	N	F	0.138	0.419	−0.168	−0.389	10.49[g]
12	O	O	0.092	0.440	−0.266	−0.266	10.75
13a	N^+		0.658	0.433	−0.091		10.97[h]

[a] Methine proton ^{1}H NMR signal (ppm) vs. internal Me_4Si in $CDCl_3$ if not otherwise stated. The samples were run at ~0.05 M. [b] Not measured. [c] In C_6D_6. [d] Central metal Ru instead of Os. [e] NO^+ linear, NO^- bent (see Table III). [f] Value of Os(OEP)NO($OClO_3$) (**10**). [g] Value of Os(OEP)N(OMe) (**11**). [h] Value of Os(OEP)N($OClO_3$) (**13**).

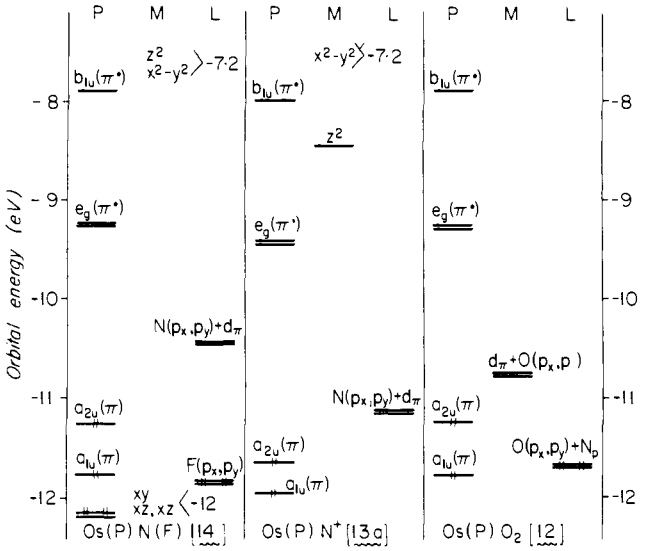

Figure 8. Energies of top filled and lowest empty MOs for complexes Os(P)L(L′) **14** and **12** and for Os(P)N^+ (**13a**). The orbitals are presented as in Figure 6.

triplet is $T_1(\pi,l_{\pi^*})$ rather than $T_1(\pi,\pi^*)$; a CT triplet may be expected to have faster radiationless decay.

Figure 8 shows calculations on three Os^{VI} complexes. Here the d_{xy}, d_π orbitals are below the energy of the diagrams. An antibonding-type orbital involving the ligands is now available for (π,l_{π^*}) transitions, and Figures 7 and 8 explain the close relation of the Os^{II} complex **10** and the Os^{VI} complex **11**, as discussed in the previous section.

Table VII gives electronic populations, based on a Mulliken population analysis,[11] for the total π electron system. We have taken this as consisting of the C(p_z), N(p_z) orbitals of the ring, Os(d_π) orbitals, and any π-type orbitals on the L(L′) ligands. Thus NH_3 and $P(OMe)_3$ are taken as having no π orbitals; for CO, CS, NO^+, N, O, and F the π orbitals are taken as p_x, p_y; for pyridine the π orbitals are taken as C(p_y), N(p_y) since the pyridine molecule was located in the *xz* plane.[7] We omit complexes with OMe^- and NO^- (bent) ligands because the low symmetry makes it difficult to define the π system. Columns 4, 5, 6, and 7 of Table VII give the π populations of the porphine ring, the two ligands L(L′), and Os(d_π), respectively. Column 8 gives the sum of columns 4–7, while column 9 gives the formal number of valence electrons expected in the π system. The Os(p_z) orbital is also part of the π system, but we list its population separately as it should also contain electron density from axial ligand σ donation.

Before discussing the trends in Table VII we should note some theoretical points. In a totally planar system, such as Cu(P) or Ag(P), the π system rigorously separates from the σ system. The total π population, including the metal p_z orbital, adds up to the number of valence electrons within round-off errors. We include numbers for Cu(P), Ag(P), and $Ag(P)^+$ for comparison.[1] The presence of fifth and sixth ligands breaks down σ,π separation. Nonetheless the π system—extending from the ring, through Os(d_π), and onto ligand π—maintains its electron population close to the number of valence electrons, as shown in Table VII.

The point of Table VII is the following. The IEH calculations show a reciprocation between *equatorial* and *axial* back-bonding which is apparent from the π population analysis. Thus **1** shows transfer from Os(d_π) into P(π) (P ≡ porphine). The *trend* from **1** to **13** is to shift density out of P(π) and out of Os(d_π) into L(π) and L′(π), a trend that crosses smoothly from Os^{II} to Os^{VI} complexes.

Total charge densities for ring, metal, and ligands are given in Table VIII. It can be seen that the trend across the BB–CT series is to shift electron density from the ring and from the metal onto the axial ligands. It is interesting to note that, as the porphyrin ring charge density increases from −0.842 to +0.658 (Table VIII), the energy of the top filled π orbitals decreases slightly (see Figures 6–8), and, as the charge on the metal increase from 0.212 to 0.433, the top filled d orbital energies decrease strongly. In this way we can understand why the first oxidation occurs at the metal for the early members of the BB–CT series and for the later members of the series the first oxidation occurs at the ring.

^{1}H NMR Chemical Shifts of the Meso Protons. It has been noted that the meso-proton resonance of metallooctaethylporphyrins depend on the oxidation state of the central metal, with δ tending to rise with higher metal valence.[24] Qualitatively, this is consistent with deshielding at the meso protons (i.e., δ rises) as higher valent metals withdraw electron density from the ring. This trend is also apparent in the series of osmium octaethylporphyrins treated here, with the optically determined BB–CT series being well reproduced by the increase of the δ_{meso} ^{1}H NMR shifts displayed in Table VIII; we see that the calculated charge densities on the porphyrin ring tend to decrease with the red shifts along the BB–CT series and with the increase of ^{1}H NMR δ_{meso} values.

While the calculated charge densities tend to increase across the BB–CT series, some discrepancies in Table VIII deserve comment: (1) For Os(OEP)[$P(OMe)_3$]$_2$ (**3**), the calculated

porphyrin ring charge density is too negative for its position in the series. Possibly if 3d orbitals were included on the P atom, this anomaly would be corrected. (2) The cation **10a**, used to model Os(OEP)NO($OClO_3$) (**10**), has too high a calculated porphyrin ring charge density for the position of **10** in the BB-CT series; on the other hand, the cation **13a**, used to model Os(OEP)N($OClO_3$) (**13**), gives a more appropriate porphyrin charge density for the position of **13** at the end of the BB-CT series. It is possible that the perchlorate of **10** is coordinated in solution so that the ionic approximation of **10** by **10a** is somewhat exaggerated; however, it may be that **13** dissociated in $CDCl_3$ to **13a** and ClO_4^-. (3) The calculated charge densities predict that $Os(OEP)O_2$ (**12**) should precede Os(OEP)N(F) (**14**) in the BB-CT series, whereas the optical data and ^1H NMR δ_{meso} values give a reverse order. Obviously the calculations are not sufficiently subtle to work out the distinction of these Os^{VI} derivatives.

Conclusion

The essential points of the back-bonding charge-transfer (BB-CT) series as elaborated here can be expressed in a rule which was named "rule of bathochromism" elsewhere:[9c,25] "In a metalloporphyrin containing filled d_π orbitals capable of back-bonding, a bathochromic shift of the α-band results if a given axial ligand is replaced by a new one with a larger π-acceptor capacity". As is shown here, this rule can be extended to metal ions that are themselves d_π acceptors, because it does not matter where the electrons populating the d_π orbitals come from. The rule of bathochromism and its product, the BB-CT series, are not restricted to osmium porphyrins, but can be traced with all sorts of metalloporphyrins of the spectral hypso or hyper type.[4] The rule seems especially useful for identifying new porphyrin complexes in which the coordination of a certain axial ligand with known π-acceptor capacity is suspected, e.g., novel hemes or heme models.[25]

Finally it should be noted that Spiro and Burke[26] found an effect in resonance Raman studies of complexes Fe(MP)L(L′) (MP = mesoporphyrin IX dimethyl ester) essentially like the BB-CT series: "Axial ligands of increasing π acid strength bound to Fe^{II} hemes progressively increase the frequency of the "oxidation state" marker bands". This increase in frequency of the ring oxidation state marker bands is attributed to a shift of electrons from the ring $e_g(\pi^*)$ orbital to the axial ligand l_{π^*} orbital. We then predict that complexes (Os(OEP)-L(L′) will also show ring oxidation state marker bands that will increase in frequency from compound **1** to **13**. The fact that the BB-CT series naturally accounts for the marker bands noted by Spiro and Burke further suggests that these same considerations play a role in the functioning of heme proteins.

References and Notes

(1) Part 38: A. Antipas, D. Dolphin, M. Gouterman, and E. C. Johnson, *J. Am. Chem. Soc.*, **100**, 7705 (1978). Part 39 is at the same time part 21 of the series "Metal Complexes of Tetrapyrrole Ligands" issued at Aachen and Darmstadt. Part 20: ref 7. Part 19: ref 9c.

(2) (a) University of Washington, Seattle; (b) Technische Hochschule, Aachen; (c) Department of Chemistry, University of British Columbia, Vancouver, B.C. V6T 1W5, Canada; (d) Eduard-Zintl-Institut, Anorganische Chemie, D-61 Darmstadt, West Germany.

(3) J. W. Buchler in "Porphyrins and Metalloporphyrins", K. M. Smith, Ed., Elsevier, Amsterdam, 1975, Chapter 5, p 157.

(4) J. W. Buchler, W. Kokisch, and P. D. Smith, *Struct. Bonding (Berlin)*, **34**, 79 (1978).

(5) J. W. Buchler in "The Porphyrins", Vol. I, D. Dolphin, Ed., Academic Press, New York, 1978, Chapter 10, p 389.

(6) M. Gouterman in ref 5, Vol. III, Chapter 1, p 1.

(7) Part 36: A. Antipas, J. W. Buchler, M. Gouterman, and P. D. Smith, *J. Am. Chem. Soc.*, **100**, 3015 (1978).

(8) P. D. Smith, Doctoral Dissertation, Technische Hochschule, Aachen, 1976.

(9) (a) J. W. Buchler and K. Rohbock, *J. Organomet. Chem.*, **65**, 223 (1974); (b) J. W. Buchler and P. D. Smith, *Chem. Ber.*, **109**, 1465 (1976); (c) J. W. Buchler, W. Kokisch, P. D. Smith, and B. Tonn, *Z. Naturforsch. B*, **33**, 1371 (1978).

(10) Part 31: M. Gouterman, L. K. Hanson, G.-E. Khalil, J. W. Buchler, K. Rohbock, and D. Dolphin, *J. Am. Chem. Soc.*, **97**, 3142 (1975).

(11) Part 4: M. Zerner and M. Gouterman, *Theor. Chim. Acta*, **4**, 44 (1966).

(12) Part 28: A. M. Schaffer, M. Gouterman, and E. R. Davidson, *Theor. Chim. Acta*, **30**, 9 (1973).

(13) L. K. Hanson, W. A. Eaton, S. G. Sligar, I. C. Gunsalus, M. Gouterman, and C. R. Connell, *J. Am. Chem. Soc.*, **98**, 2672 (1976).

(14) L. C. Cusachs and J. H. Corrington in "Sigma Molecular Orbital Theory", O. Sinanoglu and K. B. Wiberg, Eds., Yale University Press, New Haven, Conn., 1970, pp 256–272.

(15) S. P. McGlynn, L. G. Vanquickenborne, M. Kinoshita, and D. G. Carroll, "Introduction to Applied Quantum Chemistry", Holt, Rinehart and Winston, New York, 1972, pp 106–113.

(16) Part 21: A. M. Schaffer and M. Gouterman, *Theor. Chim. Acta*, **18**, 1 (1970).

(17) B. B. Wayland and L. W. Olson, *J. Am. Chem. Soc.*, **96**, 6037 (1974).

(18) Part 18: D. Eastwood and M. Gouterman, *J. Mol. Spectrosc.*, **35**, 359 (1970).

(19) Part 27: M. Gouterman, F. P. Schwarz, P. D. Smith, and D. Dolphin, *J. Chem. Phys.*, **59**, 676 (1973). Addendum: M. Gouterman and D. B. Howell, *ibid.*, **61**, 3491 (1974).

(20) Part 29: L. K. Hanson, M. Gouterman, and J. C. Hanson, *J. Am. Chem. Soc.*, **95**, 4822 (1973).

(21) T. L. Hill, "An Introduction to Statistical Thermodynamics", Addison-Wesley, Reading, Mass., 1960, Chapter 22.

(22) **1** has not been studied for emission, but we predict that none will be observed.

(23) Part 32: M. Gouterman, L. K. Hanson, G.-E. Khalil, W. R. Leenstra, and J. W. Buchler, *J. Chem. Phys.*, **62**, 2343 (1975).

(24) H. Scheer and J. J. Katz in ref 3, Chapter 10, p 460–462.

(25) J. W. Buchler, *Angew. Chem., Int. Ed. Engl.*, **17**, 407 (1978).

(26) T. G. Spiro and J. M. Burke, *J. Am. Chem. Soc.*, **98**, 5482 (1976).